

# TE-Case RCS Analysis of Finite-Thickness Slotted Circular Cylinder Loaded With Lossy Filling

Andriy E. Serebryannikov, *Member, IEEE*, and Alexander I. Nosich, *Fellow, IEEE*

**Abstract**—A generalized model is developed to study the TE-polarized plane wave scattering by coated and uncoated slotted circular cylinders of nonzero thickness and by a filled and not filled circular cylinders with sectorial cuttings. The mathematical treatment is based on the coupled integral equations (IEs) with respect to the tangential electric field at the slot/cutting apertures. The Galerkin method with weighted Gegenbauer polynomials as basis functions is used to convert IEs to a set of linear algebraic equations. Numerical simulations of the radar cross section (RCS) are carried out in the case of single slot/cutting in order to reveal the effect of thickness. Potentials of three approximations to the field in the slot/cutting domain are studied. Their use enables one to substantially accelerate the RCS calculations.

**Index Terms**—Cavity-backed aperture (CBA), coating, Galerkin method, radar cross section (RCS), slot.

## I. INTRODUCTION

**S**CATTERING of plane electromagnetic waves by and penetration into cavity-backed apertures (CBA) have been extensively investigated during the past two decades. It was mainly motivated by the applications such as control of radar cross section (RCS), shielding electromagnetically-sensitive enclosures, and enhancing the compatibility of microwave systems. This problem has been studied for different two-dimensional (2-D) cylindrical structures, by many authors with the aid of various analytical [1], numerical [2]–[11], and approximate asymptotic approaches [12]–[17]. An efficient analytical (perturbational) approach, the resonant mode expansion, was developed in [1]. A lot of numerical studies devoted to CBA have been carried out by applying IE [2]–[10] and the mode-matching [11] techniques. The most efficient, analytical regularization (preconditioning) approach combining analytical and numerical techniques was used in [13]–[17].

The afore-mentioned approaches have been applied to various CBA geometries, whose far and near-field characteristics were calculated. In the most cases, infinitely thin cylindrical shells with and without interior filling have been studied: circular shells [1], [7], [9], [14], [15], rectangular shells [7], [10], and arbitrary shape shells [5], [6], [8]. In [2] the interior of multiple-aperture circular shell presented a finite number of material layers and concentric shells with multiple apertures. A great attention has been also paid to the structures containing inner

or/and outer lossy coatings [3], [12], [16], [17] used for damping the potentials of RCS resonances. The other type of the CBA shaped as a circular conducting cylinder with the sectorial cutting was considered in [4]. Cylindrical structures with nonzero thickness and without coating were studied in [8], [11].

The main aim of this work is to develop an approach able to describe a wide class of CBA of the circular and sectorial geometries of the inner cavity, with an account of nonzero thickness of the shell, multiple apertures, and lossy coating. Hence, our model covers much wider class of CBA than those studied before. Our approach is close to that used in [18] for calculations of cutoff wavenumbers of a ridge circular waveguide with nonzero thickness of the ridges. As in [18], we use here the coupled IEs technique and the Galerkin method to obtain the set of linear algebraic equations. It is well-known that the efficiency of a solution for the structure showing the edges strongly depends on whether a specific behavior of the field at the edges is taken into account. To do this, appropriate basis functions should be used when applying the Galerkin method. The weighted cosine functions were employed in [18]. However, the use of the weighted orthogonal polynomials as basis functions is considered to be more appropriate. For example, the weighted Chebyshev polynomials [19] of the first kind have been used in [2], [3] in the case of infinitely thin shell. Since in our case the thickness is nonzero, it is the most appropriate to use the Gegenbauer polynomials [19].

We develop a theory, which treats geometry with arbitrary (nonzero) thickness of the metallic shell, and apply it to numerical study of the thickness effect on dependences of RCS on frequency and geometrical parameters (GPs). The paper is organized as follows. In Section II, we present the general formulation of the problem and three approximations to the field in the slot/cutting domain. Sample numerical results are presented and discussed in Section III in special case of a single slot/cutting. The frequency, slot/cutting aperture angle, and shell thickness dependences of RCS are presented there, and demonstrate interesting features. Special attention is paid to the study of potentials of the approximate solutions based on the above-mentioned approximations. The paper is finished with a short conclusion.

## II. THEORY

### A. Problem Formulation

Fig. 1(a) shows a generic geometry, which corresponds to a PEC finite-thickness cylinder with the inner radius  $\rho_2$  and the outer radius  $\rho_3$ . The cylinder has  $N$  slots. The symmetry axis of

Manuscript received May 19, 2003; revised July 30, 2004.

A. E. Serebryannikov was with the Institute of Radio Astronomy, National Academy of Sciences of Ukraine, 61002 Kharkov, Ukraine. He is now with the Technische Universitaet Hamburg-Harburg, D-21071 Hamburg, Germany (e-mail: asecerbr@hotmail.com; serebryannikov@tu-harburg.de).

A. I. Nosich is with the Institute of Radio Physics and Electronics, National Academy of Sciences of Ukraine, 61085 Kharkov, Ukraine.

Digital Object Identifier 10.1109/TAP.2005.844455

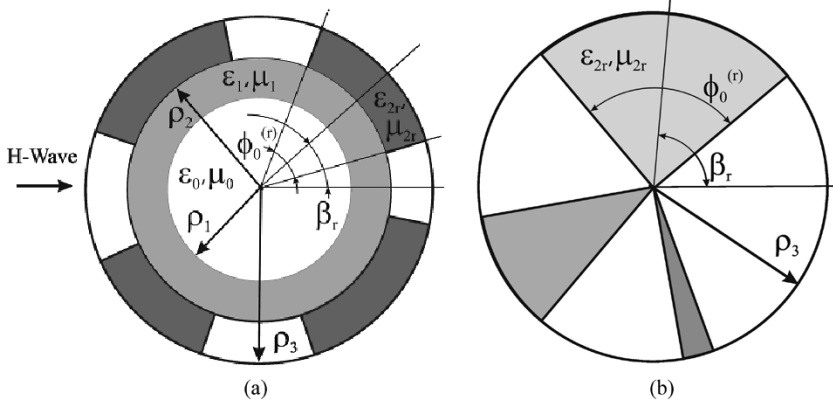


Fig. 1. Geometry of the structures studied: (a) slotted circular metallic shell of nonzero thickness coated with lossy material from inside and with the sectorial cuttings filled with lossy materials. In case (a), the slots filled with a lossy material and the lossy inner coating are shown by more and less dark half-tones of grey, respectively. In case (b), different half-tones correspond to different lossy materials filling sectorial cuttings. PEC segments at  $\rho_2 \leq \rho \leq \rho_3$  (a) and at  $\rho \leq \rho_3$  (b) are shown in white.

a slot and its angular dimension are noted by  $\beta_r$  and  $\phi_0^{(r)}$ , respectively,  $r = 1, 2, \dots, N$ . There is a lossy inner coating with relative material parameters  $\epsilon_1$  and  $\mu_1$ , which occupies the domain  $\rho_1 \leq \rho \leq \rho_2$ . The slot domain,  $\rho_2 \leq \rho \leq \rho_3, \beta_r - \phi_0^{(r)}/2 \leq \phi \leq \beta_r + \phi_0^{(r)}/2$  is filled in with a lossy material characterized by the relative parameters  $\epsilon_{2r}$  and  $\mu_{2r}$ . A special case is shown in Fig. 1(b), that is a circular cylinder whose  $N$  sectorial cuttings are filled in with the lossy materials. This case is obtained from the general one by setting  $\rho_1 = \rho_2 = 0$ .

The structure is illuminated by the plane wave as shown in Fig. 1 ( $\phi_{\text{inc}} = \pi$ ). The time dependence  $\exp(i\omega t)$  has been assumed and suppressed throughout the paper. In the general case,  $H_z$  component at  $\rho \leq \rho_1$  (domain I) is expanded as follows:

$$H_z^I = \sum_{m=0}^{\infty} (A_m^c \cos m\phi + A_m^s \sin m\phi) J_m(k_0\rho) \quad (1)$$

where  $k_0$  is the free-space wavenumber. In the coating (domain II), it is expanded as

$$H_z^{II} = \sum_{m=0}^{\infty} [(B_m^c \cos m\phi + B_m^s \sin m\phi) J_m(k_1\rho) + (C_m^c \cos m\phi + C_m^s \sin m\phi) Y_m(k_1\rho)]. \quad (2)$$

In the slots (domain III), we have

$$H_z^{III(r)} = \sum_{n=0}^{\infty} [D_{nr} J_{\nu_{nr}}(k_2^{(r)}\rho) + E_{nr} Y_{\nu_{nr}}(k_2^{(r)}\rho)] \cos[\nu_{nr}(\phi - \tilde{\phi}_r)] \quad (3)$$

and, finally, in the outer space (domain IV),  $H_z$  is presented as a sum of the incident and scattered fields as follows:

$$H_z^{IV} = \exp(-ik_0\rho \cos \phi) + \sum_{m=0}^{\infty} (F_m^c \cos m\phi + F_m^s \sin m\phi) H_m^{(2)}(k_0\rho). \quad (4)$$

In (1)–(4),  $A_m^{c,s}, B_m^{c,s}, C_m^{c,s}, F_m^{c,s}, D_{nr}$ , and  $E_{nr}$  are unknown coefficients, which represent the amplitudes of the space harmonics, whose upper indices  $c$  and  $s$  indicate the cosine and sine dependence in  $\phi$ , respectively;  $J_h, Y_h$ , and  $H_h^{(2)}$  are the  $h$ th order Bessel, Neumann, and second-kind Hankel functions, respectively;  $k_1 = k_0\sqrt{\epsilon_1\mu_1}$  and  $k_2^{(r)} = k_0\sqrt{\epsilon_{2r}\mu_{2r}}$  are the wavenumbers in the inner coating and slot domains, respectively;  $\tilde{\phi}_r = \beta_r - \phi_0^{(r)}/2$ ; the index of cylindrical functions in each slot domain,  $\nu_{nr} = \pi n/\phi_0^{(r)}$ , is chosen in such a manner that  $E_\rho$  vanishes at the walls of the slot, i.e., at  $\phi = \beta_r \pm \phi_0^{(r)}/2$ .

### B. Basic Equations for Arbitrary Shell

In order to find the unknown coefficients in (1)–(4), the boundary conditions are used. First of all, let satisfy the continuity of the  $E_\phi$  component on the slot openings, i.e., at  $\beta_r - \phi_0^{(r)}/2 \leq \phi \leq \beta_r + \phi_0^{(r)}/2, r = 1, 2, \dots, N, \rho = \rho_2, \rho_3$ , and the vanishing of  $E_\phi$  at the PEC segments,  $\beta_r + \phi_0^{(r)}/2 \leq \phi \leq \beta_h - \phi_0^{(h)}/2, h = r+1 \text{ at } r = 1, 2, \dots, N-1 \text{ and } h = 1 \text{ at } r = N$ . We use the boundary conditions at  $\rho = \rho_1$  in order to exclude the coefficients  $C_m^{c,s}$  from further consideration. This yields

$$C_m^{c,s} = -K_m B_m^{c,s} \quad (5)$$

where

$$K_m = [J_m(k_1\rho_1) - \tau_m J'_m(k_1\rho_1)] / [Y_m(k_1\rho_1) - \tau_m Y'_m(k_1\rho_1)] \quad (6)$$

$\tau_m = (W_1/W_0)J_m(k_0\rho_1)/J'_m(k_0\rho_1)$ ,  $J'_m$  and  $Y'_m$  are the derivatives of the corresponding functions with respect to the arguments,  $W_0 = \sqrt{\mu_0/\epsilon_0}$  and  $W_1 = \sqrt{\mu_1/\epsilon_1}$  are the wave impedances of the free space and the coating/filling material, respectively.

Now introduce two auxiliary functions for each slot, which represent the angular dependence of  $E_\phi$  at the inner and outer

apertures,  $\rho = \rho_2, \rho_3, \beta_r - \phi_0^{(r)}/2 \leq \phi \leq \beta_r + \phi_0^{(r)}/2, r = 1, 2, \dots, N$ , as follows:

$$E_\phi^{\text{II}}(\rho_2, \phi) = E_\phi^{\text{III}(r)}(\rho_2, \phi) = iW_0 Y^{(r)}(\phi) \quad (7)$$

$$E_\phi^{\text{IV}}(\rho_3, \phi) = E_\phi^{\text{III}(r)}(\rho_3, \phi) = iW_0 V^{(r)}(\phi). \quad (8)$$

Using the orthogonality of the sine and cosine functions, vanishing of  $E_\phi$  at the PEC segments, and relation between  $E_\phi$  and  $H_z$  components, we obtain the coefficients  $B_m^{c,s}, F_m^{c,s}, D_{nr}$ , and  $E_{nr}$ . Substituting them into expressions for  $H_z$  (1)–(4), and then into the boundary conditions on the slot apertures

$$H_z^{\text{II}}(\rho_2, \phi) = H_z^{\text{III}(r)}(\rho_2, \phi) \quad (9)$$

$$H_z^{\text{IV}}(\rho_3, \phi) = H_z^{\text{III}(r)}(\rho_3, \phi) \quad (10)$$

we obtain  $2N$  IEs with respect to unknown angular distribution of the  $E_\phi$  component at the apertures. First  $N$  of these equations take into account the geometry of the domains III and IV and characteristics of the incident wave. These equations are

$$\begin{aligned} \sum_{s=1}^N \sum_{m=0}^{\infty} R_m \Lambda_{mh}(R) - \sum_{n=0}^{\infty} \Psi_{nr} \left( \theta \tilde{X}_{\text{II}0}^{(r)} P_{nr} - \tilde{X}_{\text{II}1}^{(r)} Q_{nr} \right) \\ = - \sum_{m=0}^{\infty} (-i)^m (2 - \delta_m^0) S_m \cos m\phi \end{aligned} \quad (11)$$

where  $\delta_m^0$  is the Kronecker delta,  $r = 1, 2, \dots, N, h = 1$  and  $\theta = \rho_2/\rho_3$ . The other  $N$  equations account for the geometry of the domains I, II, and III. They are given by

$$\begin{aligned} \sum_{s=1}^N \sum_{m=0}^{\infty} T_m \Lambda_{mh}(T) - \sum_{n=0}^{\infty} \Psi_{nr} \left( \tilde{X}_{\text{II}0}^{(r)} U_{nr} - \tilde{X}_{\text{II}1}^{(r)} P_{nr} \right) = 0 \\ r = 1, 2, \dots, N, \quad h = 0. \end{aligned} \quad (12)$$

The factors  $\Psi_{nr}$  and  $\Lambda_{mh}$ , which appear in (11) and (12), depend on the angular dimension and location of corresponding slot and expressed as follows:

$$\Psi_{nr} = (2 - \delta_n^0) \cos[\nu_{nr}(\phi - \tilde{\phi}_r)] W_0 / (\phi_0^{(r)} W_2^{(r)}) \quad (13)$$

$$\begin{aligned} \Lambda_{mh}(\eta_h) = (2 - \delta_m^0) W_h (2\pi W_1)^{-1} \\ \times \left[ \cos m\phi \left( \tilde{X}_{\text{I}hc}^{(s)} \cos m\beta_s - \tilde{X}_{\text{I}hs}^{(s)} \sin m\beta_s \right) \right. \\ \left. + \sin m\phi \left( \tilde{X}_{\text{I}hc}^{(s)} \sin m\beta_s + \tilde{X}_{\text{I}hs}^{(s)} \cos m\beta_s \right) \right] \end{aligned} \quad (14)$$

where  $\eta_h = T$  at  $h = 0$  and  $\eta_h = R$  at  $h = 1$ , and  $W_2^{(r)} = \sqrt{\mu_{2r}/\varepsilon_{2r}}$ . The factors  $R_m, S_m$ , and  $T_m$  taking into account the radial composition of the shell are given by  $R_m = H_m^{(2)}(k_0\rho_3)/H_m^{(2)'}(k_0\rho_3), S_m = J_m(k_0\rho_3) - J_m'(k_0\rho_3)R_m, T_m = [J_m(k_1\rho_2) - K_m Y_m(k_1\rho_2)]/[J_m'(k_1\rho_2) - K_m Y_m'(k_1\rho_2)]$ . The factors depending on the radial geometry of the slots are given by  $U_{nr} = Z_{\nu_{nr}}(k_2^{(r)}\rho_2, k_2^{(r)}\rho_3)/\tilde{Z}_{\nu_{nr}}(k_2^{(r)}\rho_2, k_2^{(r)}\rho_3)$

$$P_{nr} = 2 / \left[ \pi k_2^{(r)} \rho_2 \tilde{Z}_{\nu_{nr}}(k_2^{(r)}\rho_2, k_2^{(r)}\rho_3) \right] \quad \text{and}$$

$$Q_{nr} = Z_{\nu_{nr}}(k_2^{(r)}\rho_3, k_2^{(r)}\rho_2) / \tilde{Z}_{\nu_{nr}}(k_2^{(r)}\rho_2, k_2^{(r)}\rho_3)$$

where  $Z_{\nu_{nr}}(x_1, x_2) = J_{\nu_{nr}}(x_1)Y'_{\nu_{nr}}(x_2) - Y_{\nu_{nr}}(x_1)J'_{\nu_{nr}}(x_2)$  and  $\tilde{Z}_{\nu_{nr}}(x_1, x_2) = d[Z_{\nu_{nr}}(z, x_2)]/dz|_{z=x_1}$ . The factors  $\tilde{X}_{\text{II}0c,s}^{(s)}$  are given by

$$\tilde{X}_{\text{II}0c,s}^{(s)} = \int_{-a_s}^{a_s} Y^{(s)}(\phi'_s) \Phi_m^{cs}(\phi'_s) d\phi'_s \quad (15)$$

where  $\Phi_m^c(\phi'_s) = \cos m\phi'_s, \Phi_m^s(\phi'_s) = \sin m\phi'_s, a_s = \phi_0^{(s)}/2$  while  $\phi'_s = 0$  of the local coordinate system corresponds to the symmetry axis of the  $s$ th slot, i.e.,  $\phi'_s = \phi_{\text{local}} = \phi - \beta_s$ .  $\tilde{X}_{\text{II}1c,s}^{(s)}$  is obtained from (15) where  $Y^{(s)}$  is replaced by  $V^{(s)}$ . The factors  $\tilde{X}_{\text{II}10}^{(r)}$  are given by

$$\tilde{X}_{\text{II}10}^{(r)} = \int_{-a_r}^{a_r} Y^{(r)}(\phi'_r) \cos [\nu_{nr}(\phi'_r + a_r)] d\phi'_r. \quad (16)$$

$\tilde{X}_{\text{II}11}^{(r)}$  is given by (16) where  $Y^{(r)}$  is replaced by  $V^{(r)}$ .

In order to convert (11), (12) into the set of algebraic equations, we apply the Galerkin method. Thus, we express  $Y^{(s)}(x)$  and  $V^{(s)}(x)$  as follows:

$$Y^{(s)}(x) = \sum_{i=1}^M c_{is} \Theta_{is}(x) \quad (17)$$

$$V^{(s)}(x) = \sum_{i=1}^M d_{is} \Theta_{is}(x) \quad (18)$$

where  $c_{is}$  and  $d_{is}$  are unknown coefficients,  $\Theta_{is}(x)$  are the basis functions, which take into account the field behavior at the edges.

Substituting (17), (18) into (11), (12), multiplying them with  $\Theta_{jr}$  for each  $r$ , and then integrating over  $\phi$  at the range from  $-a_r$  to  $a_r$ , we arrive after some manipulations at the following set of linear algebraic equations with respect to the coefficients  $c_{is}$  and  $d_{is}$ :

$$\begin{aligned} \sum_{i=1}^M \sum_{s=1}^N \delta_r^s \sum_{n=0}^{\infty} L_{nr} [c_{ir}(\theta P_{nr} + U_{nr}) - d_{ir}(Q_{nr} + P_{nr})] \\ - c_{is} \Omega_{isjr}(T) - d_{is} \Omega_{isjr}(R) = A_{jr} \end{aligned} \quad (19)$$

$$\begin{aligned} \sum_{i=1}^M \sum_{s=1}^N \delta_r^s \sum_{n=0}^{\infty} L_{nr} [c_{ir}(\theta P_{nr} - U_{nr}) - d_{ir}(Q_{nr} - P_{nr})] \\ + c_{is} \Omega_{isjr}(T) - d_{is} \Omega_{isjr}(R) = A_{jr}. \end{aligned} \quad (20)$$

Here,  $r = 1, 2, \dots, N, j = 1, 2, \dots, M$

$$L_{nr} = (2 - \delta_n^0) W_0 \tilde{\Theta}_{ir}^{\text{II}} \tilde{\Theta}_{jr}^{\text{II}} / \left( \phi_0^{(r)} W_2^{(r)} \right) \quad (21)$$

$$\begin{aligned} A_{jr} = \sum_{m=0}^{\infty} (2 - \delta_m^0) (-i)^m S_m \\ \times \left( \tilde{\Theta}_{jr}^{\text{I}c} \cos m\beta_r - \tilde{\Theta}_{jr}^{\text{I}s} \sin m\beta_r \right) \end{aligned} \quad (22)$$

$$\begin{aligned} \Omega_{isjr}(X) = \varsigma \left\{ X_0 \tilde{\Theta}_{is}^{\text{I}c} \tilde{\Theta}_{jr}^{\text{I}c} / 2 \right. \\ \left. + \sum_{m=1}^{\infty} X_m \left[ \left( \tilde{\Theta}_{is}^{\text{I}c} \tilde{\Theta}_{jr}^{\text{I}c} + \tilde{\Theta}_{is}^{\text{I}s} \tilde{\Theta}_{jr}^{\text{I}s} \right) \cos m\gamma_{rs} \right. \right. \\ \left. \left. + \left( \tilde{\Theta}_{is}^{\text{I}c} \tilde{\Theta}_{jr}^{\text{I}s} - \tilde{\Theta}_{is}^{\text{I}s} \tilde{\Theta}_{jr}^{\text{I}c} \right) \sin m\gamma_{rs} \right] \right\} \end{aligned} \quad (23)$$

where  $\gamma_{rs} = \beta_s - \beta_r$ ,  $\varsigma = 1/\pi$  if  $X = R$  and  $\varsigma = W_0/(\pi W_1)$  if  $X = T$

$$\tilde{\Theta}_{is}^{Ic,s} = \int_{-a_s}^{a_s} \Theta_{is}(\phi'_s) \Phi_m^{c,s}(\phi'_s) d\phi'_s \quad (24)$$

$$\tilde{\Theta}_{ir}^{II} = \int_{-a_r}^{a_r} \Theta_{ir}(\phi'_r) \cos[\nu_{nr}(\phi'_r + a_r)] d\phi'_r. \quad (25)$$

We use here

$$\Theta_{ir}(x) = [1 - (x/a_r)^2]^{-1/3} G_{i-1}^{1/6}(x/a_r) \quad (26)$$

where  $G_{i-1}^{1/6}$  is the Gegenbauer polynomial of the order  $i - 1$  [19]. In this case,  $\tilde{\Theta}_{ir}^{II} \tilde{\Theta}_{jr}^{II} = (-1)^{n-1+(i+j)/2} a_r^2 \vartheta_{i-1}(\pi n/2) \vartheta_{j-1}(\pi n/2)$  if  $n, i - 1$ , and  $j - 1$  are simultaneously either even or odd, and  $\tilde{\Theta}_{ir}^{II} \tilde{\Theta}_{jr}^{II} = 0$  otherwise. At odd  $i$ ,  $\tilde{\Theta}_{is}^{Ic} = (-1)^{(i-1)/2} a_s \vartheta_{i-1}(ma_s)$  and  $\tilde{\Theta}_{is}^{Is} = 0$ . At even  $i$ ,  $\tilde{\Theta}_{is}^{Is} = (-1)^{i/2-1} a_s \vartheta_{i-1}(ma_s)$  and  $\tilde{\Theta}_{is}^{Ic} = 0$ . The factors  $\vartheta_i(x)$  are given by  $\vartheta_i(x) = 2\pi\Gamma(i + 1/3)\varphi(i, x)/[i!\Gamma(1/6)]$  where  $\varphi(i, x) = (2x)^{-1/6} J_{i+1/6}(x)$  if  $x \neq 0$  and  $\varphi(i, x) = \delta_i^0/[2^{1/3}\Gamma(7/6)]$  if  $x = 0$ , and  $\Gamma$  is gamma function.

If there is no inner coating, one should use  $T_m = J_m(k_0\rho_2)/J'_m(k_0\rho_2)$ . In the case of sectorial geometry shown in Fig. 1(b), one should assume that  $\rho_2 = 0$ . Then we obtain, instead of (19) and (20), a single equation

$$\sum_{i=1}^M \sum_{s=1}^N d_{is} \left[ \delta_r^s \sum_{n=0}^{\infty} L_{nr} w_{nr} - \Omega_{isjr}(R) \right] = A_{jr} \quad (27)$$

where  $j = 1, 2, \dots, M$ ;  $r = 1, 2, \dots, N$ , and  $w_{nr} = J_{\nu_{nr}}(k_2^{(r)}\rho_3)/J'_{\nu_{nr}}(k_2^{(r)}\rho_3)$ .

### C. Expression for RCS

Once the coefficients  $c_{ir}, d_{ir}$  are found, the backscattering cross section is calculated as

$$\sigma = \lim_{\rho \rightarrow \infty} 2\pi\rho \left[ |H_z^{\text{sc}}(\rho, \pi)|^2 / |H_z^{\text{inc}}|^2 \right] \quad (28)$$

where  $|H_z^{\text{inc}}|$  is the amplitude of the incident field, which is assumed to be 1

$$H_z^{\text{sc}}(\rho, \pi) = \sum_{m=0}^{\infty} (-1)^m F_m^c H_m^{(2)}(k_0\rho) \quad (29)$$

with

$$\begin{aligned} F_m^c &= (2 - \delta_m^0) \left[ -(-i)^m J_m'(k_0\rho_3) + (2\pi)^{-1} \right. \\ &\quad \times \sum_{i=1}^M \sum_{s=1}^N d_{is} \left( \tilde{\Theta}_{is}^{Ic} \cos m\beta_s - \tilde{\Theta}_{is}^{Is} \sin m\beta_s \right) \\ &\quad \left. \times [H_m^{(2)'}(k_0\rho_3)]^{-1} \right]. \end{aligned} \quad (30)$$

Using the large-argument asymptotic of the Hankel function [19] we obtain

$$\sigma = 4\xi(m)\xi^*(s)/k_0 \quad (31)$$

where  $\xi(h) = \sum_{h=0}^{\infty} (-i)^h F_h^c$  and the asterisk means the complex conjugate. Further we use the RCS normalized by the geometrical optics RCS value for the closed PEC cylinder

$$\tilde{\sigma} = 4\xi(m)\xi^*(s)/(\pi k_0\rho_3). \quad (32)$$

### D. Approximations

A simplified version of (19), (20) can be derived for the thin wall approximation (TWA), that is  $\delta^{(r)} \ll 1$ , where  $\delta^{(r)} = y_3^{(r)} - y_2^{(r)}, y_h^{(r)} = k_2^{(r)}\rho_h, h = 2, 3$ . In this case, all cylindrical functions in terms of  $P_{nr}, Q_{nr}$ , and  $U_{nr}$  are replaced with the first terms of their Taylor series. This results in substantial simplification of the calculation of the terms accounting for the effect of the slots. We obtain for them that

$$Q_{nr} + P_{nr} \approx 2 / \left\{ [1 - (\nu_{nr}/y_2^{(r)})^2] \delta^{(r)} \right\} \quad (33)$$

$$\theta P_{nr} + U_{nr} \approx \left( 1 - \delta^{(r)} / y_3^{(r)} \right) (Q_{nr} + P_{nr}) \quad (34)$$

$$\theta P_{nr} - U_{nr} = Q_{nr} - P_{nr} = O(\delta^{(r)}). \quad (35)$$

Another useful approximation has been obtained in the case of rather narrow slot/cutting,  $\phi_0^{(r)}/\pi \ll 1, r = 1, 2, \dots, N$ . Here, the large-order asymptotic of the cylindrical functions [19] is applied to  $P_{nr}, Q_{nr}, U_{nr}$ , and  $w_{nr}$ . If  $n > 0$ , then

$$\begin{aligned} Q_{nr} + P_{nr} &\approx -w_{nr} \left[ 1 + \left( y_2^{(r)} / y_3^{(r)} \right)^{\nu_{nr}} \right] \\ &\quad / \left[ 1 - \left( y_2^{(r)} / y_3^{(r)} \right)^{\nu_{nr}} \right] \end{aligned} \quad (36)$$

$$\theta P_{nr} + U_{nr} \approx (Q_{nr} + P_{nr}) y_2^{(r)} / y_3^{(r)} \quad (37)$$

$$\begin{aligned} Q_{nr} - P_{nr} &\approx -w_{nr} \left[ 1 - \left( y_2^{(r)} / y_3^{(r)} \right)^{\nu_{nr}} \right] \\ &\quad / \left[ 1 + \left( y_2^{(r)} / y_3^{(r)} \right)^{\nu_{nr}} \right] \end{aligned} \quad (38)$$

$$\theta P_{nr} - U_{nr} \approx (P_{nr} - Q_{nr}) y_2^{(r)} / y_3^{(r)} \quad (39)$$

$$w_{nr} \approx y_3^{(r)} / \nu_{nr}. \quad (40)$$

These expressions are obtained by neglecting the terms of the order  $\nu_{nr}^{-3}$ . The expressions for  $P_{0r}, Q_{0r}, U_{0r}$ , and  $w_{0r}$  given in Section II-B are still used in the framework of this approximation, which we refer to as the narrow slot approximation (NSA). The use of one of these two approximations enables one to avoid (TWA) or reduce (NSA) computing the cylindrical functions corresponding to the slot domains.

We will use one more approximation, which is based on the use of a single basis function in the Galerkin method ( $M = 1$ ). Thus we call it the single basis function approximation (SBFA). If  $N = 1$ , the use of SBFA allows one to obtain analytical solutions for  $c_{11}$  and  $d_{11}$ .

### III. NUMERICAL RESULTS AND DISCUSSION

Extensive computations have been carried out by using the developed theory for the structures showing a single slot/cutting. Dependences of RCS on the problem parameters have been studied. All results are presented in terms of the normalized RCS given by (32). It is assumed that  $\varepsilon_1 = \varepsilon_{21}$  and  $\mu_1 = \mu_{21}$ . We consider lossy coatings/fillings of two types, which are the

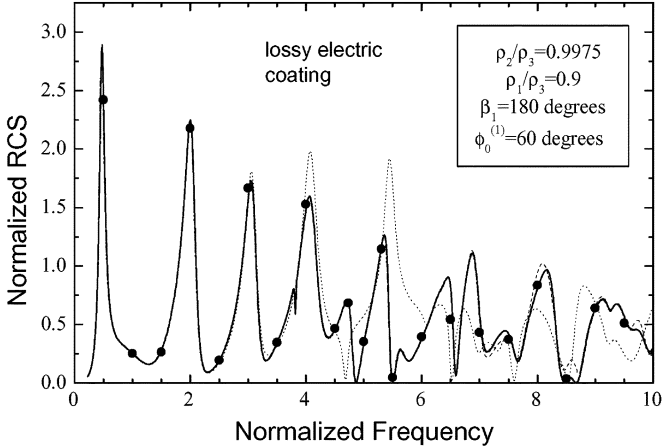


Fig. 2. Demonstration of the effect of the basis functions number on the frequency dependence of the normalized RCS. The structure shows a large aperture opening, symmetric orientation of the slot, very small thickness of the metallic shell, and is coated with lossy electric material. Dotted, dashed, dash-dotted, and solid lines correspond to  $M = 1, 3, 5$ , and  $7$ , respectively. Circles—solution for the zero-thickness cylinder ( $\rho_2/\rho_3 = 1$ ) obtained in [17] using the analytical regularization approach.

same as those considered in [16] and [17] at  $\rho_2 = \rho_3$ . Hence, the results obtained therein can be used as the entry point when studying the effect of the shell thickness. These coatings/fillings are made of shellac, natural XL ( $\varepsilon_1 = 3.45 - 0.25i$ ,  $\mu_1 = 1$ ) [20] and poly-2.5-dichlorostyrene ( $\varepsilon_1 = 7.3$ ,  $\mu_1 = 0.91 - 0.32i$ ) [12]. Further we refer to them as lossy electric and lossy magnetic coatings/fillings, respectively.

To demonstrate the effect of  $M$  on the frequency dependence of RCS, very thin metallic shell with a lossy electric coating is chosen, while the number of terms in the sums over  $m$  and  $n$  in (19), (20), (22), (23), (27), and (29) is kept rather large (Fig. 2). This metallic shell shows a geometry, which is almost the same as in [17], as it has  $\rho_2/\rho_3 = 0.9975$ . The normalized frequency is shown in units of  $k_0\rho_3$ . One can see that quite fast convergence with  $M$  occurs in the considered range of  $k_0\rho_3$ -variation. The presented results are in good agreement with those obtained in [17] for the zero-thickness shell with the aid of the analytical regularization approach. In most cases, the number of the required basis functions can be estimated as

$$M = \sqrt{|\varepsilon_1\mu_1|}k_0\rho_3 \phi_0^{(1)} / \pi + 1. \quad (41)$$

In Fig. 2, the curves obtained at  $M = 5$  and  $7$  coincide, while (41) gives  $M = 7.2$  at  $k_0\rho_3 = 10$ . Note that since symmetric orientation of the slot is considered, the even basis functions ( $i = 2h$ ,  $h = 1, 2, \dots$ ) do not affect RCS values in this case.

Fig. 3 shows dependence of the RCS versus  $k_0\rho_3$ , for three structures with rather large aperture openings, in the case of symmetric orientation of the slot. Note that the metallic shell in Fig. 3(a) shows the same geometry as that in Fig. 2. The obtained results are also in a good agreement with those obtained in [17] in the cases of magnetic coating and uncoated slotted cylinder, that confirms a possibility to apply the developed model in case of very thin shell for rather arbitrary materials (compare Figs. 2 and 3(a) with [17, Fig. 3(a)]). The main feature, which can be seen on the frequency dependence of RCS, is that sharp resonances occur that manifest themselves as extrema in the RCS. All the peaks are damped by the lossy inner coating. As a result,

the average level of RCS of coated CBA within some frequency range is much lower as compared to uncoated CBA, and even to the closed PEC cylinder. The origin of the observed resonances is explained in [16], [17], [21], [22]. One can find there several useful analytical estimates for the RCS and resonant frequencies.

Comparing the cases (a) and (b) in Fig. 3, one can see that the increase of the shell thickness leads to the shift of the extrema occurring in the frequency scan including the low-frequency peak corresponding to the shifted zero pseudo-eigenvalue [17], which is also called the Helmholtz mode [21]. However, the shift is stronger for the modes, which originate from the eigenmodes of the closed circular cylinder. Another manifestation of the effect of the increasing thickness is a substantial decrease of the average level of RCS of the coated CBA that occurs at  $k_0\rho_3 > 1$ . This is rather related to the increase of the coating thickness than to that of the shell, so far as an averaged RCS weakly depends on the shell thickness in case of uncoated CBA. The RCS value in the low-frequency resonance decreases with increase of the thickness, or even disappears if  $|k_1|$  is large enough. An interesting feature is observed near to  $k_0\rho_3 = 1$ : the larger the coating thickness, the narrower the slot, and the larger  $|k_1|$ , the closer a curve for the coated CBA to that for the closed cylinder. Thus, the effect of the interior ( $\rho \leq \rho_3$ ) is weakening and its equivalent impedance introduced at the outer aperture becomes closer to that of the PEC wall.

Results obtained for nonsymmetric ( $\beta_1 = \pi/2$ ) and back-side ( $\beta_1 = 0$ ) orientations of the slot for the structure geometry from Fig. 3(a) are also in good agreement with those obtained in [17] (see [17, Figs. 4(a) and 5(a)]). For these orientations, the thickness variation does not lead to any qualitative change in the frequency dependence. The case of  $\beta_1 = \pi/2$  shows both ranges with a slowly varying RCS-value and those with sharp extrema. In this case one can observe a growth of the maxima for the uncoated CBA while the shell thickness is decreased. An average RCS for a coated cylinder tends to that of the closed cylinder if  $k_0\rho_3 > 2$ . The larger  $|k_1|$ , the more pronounced this effect. The case with  $\beta_1 = 0$  is characterized by the decreasing of the RCS value in the low-frequency resonance and its further disappearance if the thickness increases. If  $k_0\rho_3 > 2$ , the curves obtained both for the coated and uncoated CBAs tend to coincide in average with the curve obtained for the closed cylinder.

Fig. 3(c) shows the RCS versus  $k_0\rho_3$  for the circular structure shown in Fig. 1(b) at  $N = 1$ . It is worth to note a weak effect of the inner filling in the low-frequency range: all the curves coincide there, i.e., the equivalent impedance of the interior is very close to zero in all these cases. Except for this range, the effect of the filling is stronger than for the structures with  $\rho_1 \neq 0$  and  $\rho_2 \neq 0$ .

The trends revealed in the frequency dependence of the RCS for the wide opening are observed for narrower openings as well—see Fig. 4. The decrease of  $\phi_0^{(1)}$  results in that the low-frequency resonance becomes more sensitive to the coating/filling material and the extrema shifts caused by the thickness increasing become smaller. In vicinity of  $k_0\rho_3 = 1$ , the decrease of  $\phi_0^{(1)}$  leads to the decreasing difference in RCS between the coated CBA and closed cylinder. If  $k_0\rho_3$  is rather large, the RCS for CBA with lossy electric and lossy magnetic

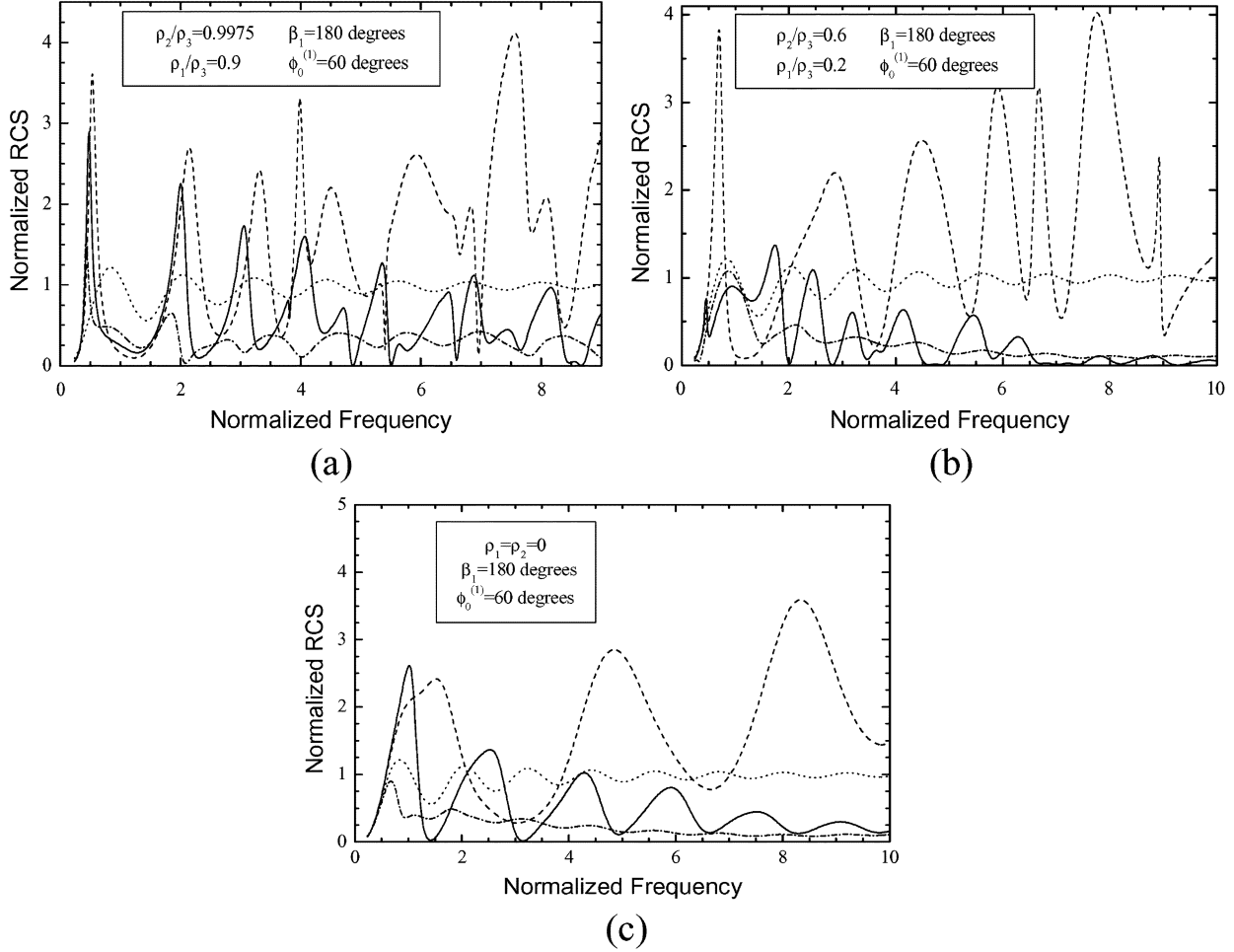


Fig. 3. Frequency dependences of the normalized RCS of CBA with wide symmetric angular aperture opening: (a) thin and (b) thick shells and (c) cylinder with the sectorial cutting. Solid, dash-dotted, dashed and dotted lines correspond to the structures with lossy electric and lossy magnetic coatings (fillings), a slotted uncoated structure, and a closed circular cylinder, respectively.

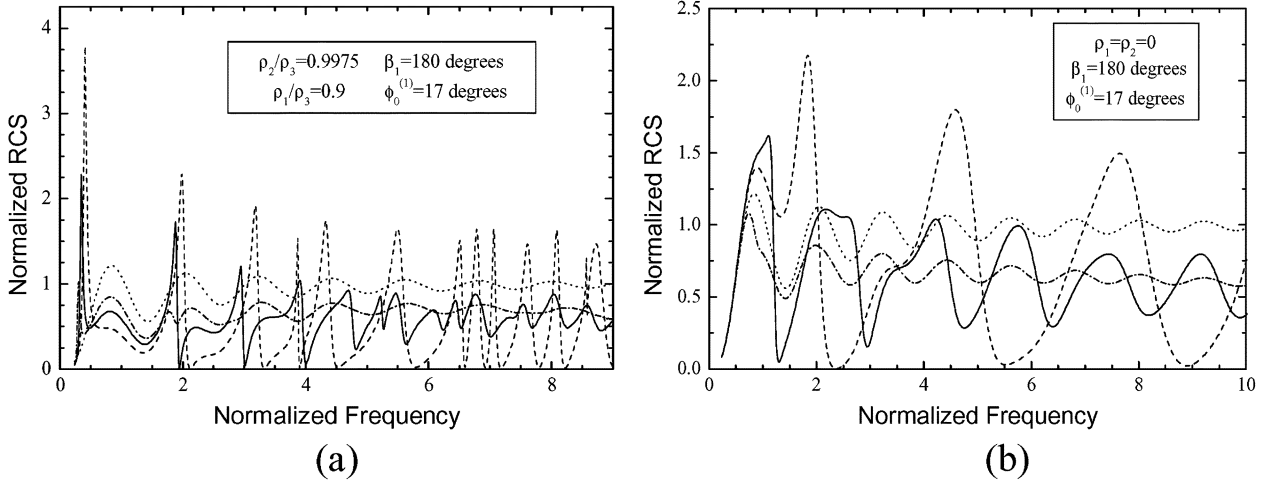


Fig. 4. Frequency dependence of the normalized RCS of CBA with narrow symmetric angular aperture opening: (a) thin shell and (b) metallic cylinder with the sectorial cutting. Solid, dash-dotted, dashed and dotted lines correspond to the structures with lossy electric and lossy magnetic coatings (fillings), a slotted uncoated structure, and a closed circular cylinder, respectively.

inner coatings apparently show a trend to coincide in average. Deep minima with near-zero values are observed for an uncoated/unfilled structure. We have to note that all the trends and features seen in Figs. 3 and 4 occur in a wide range of the variation of  $\phi_0^{(1)}$  at least from  $10^\circ$  to  $60^\circ$ .

The numerical results were obtained using a PC with AMD Athlon 1 GHz processor and 512 MB memory. CPU time required to obtain a curve in Figs. 2–4 consisting of 800 values of the RCS at  $M = 7$  is about 4 min, and can be substantially reduced if the recurrent formulas are used to calculate the combi-

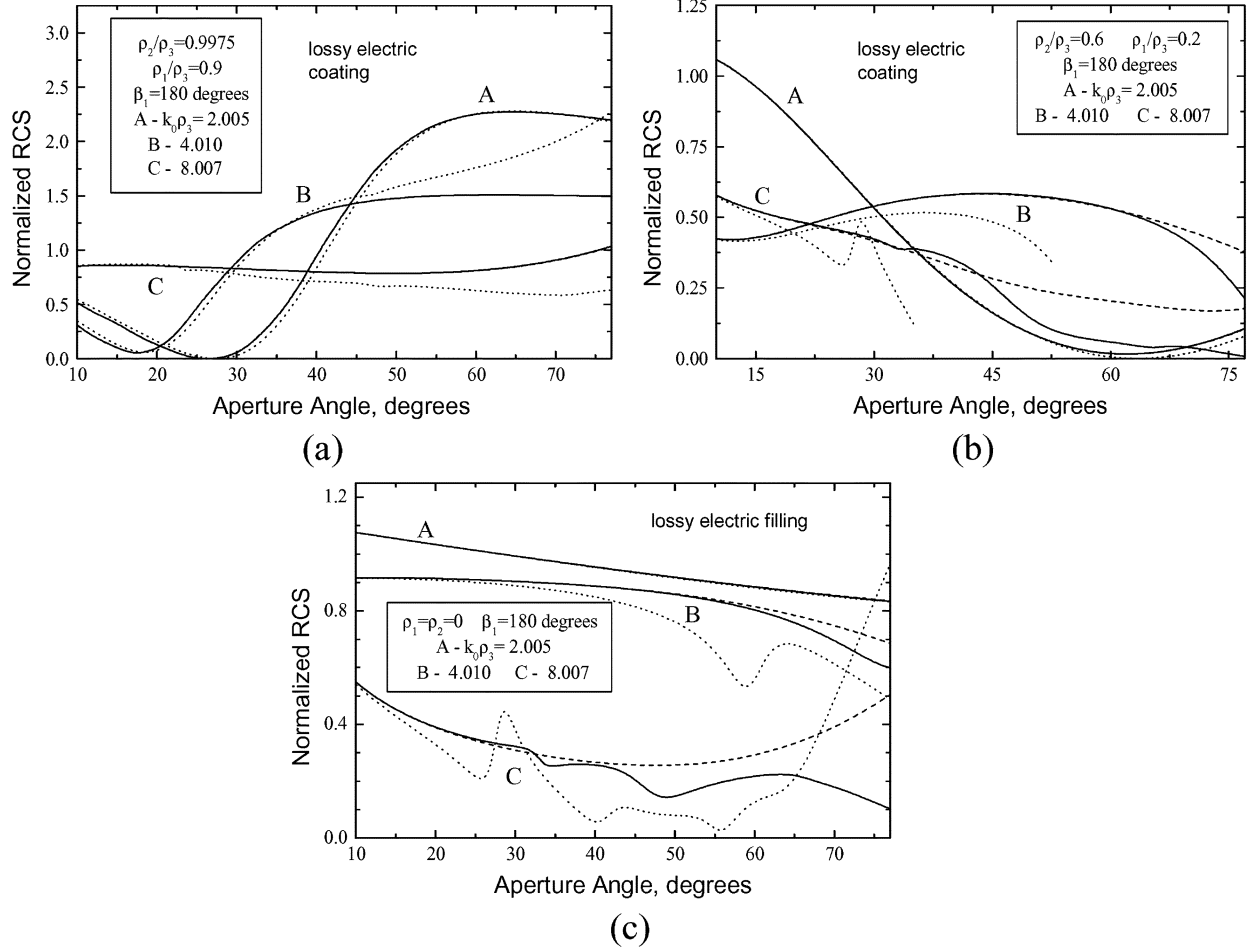


Fig. 5. Dependences of the normalized RCS on the angular size of the aperture opening for the structures with lossy electric coating (filling) having symmetric orientation: (a) thin shell, (b) thick shell, and (c) metallic cylinder with a cutting. Solid, dashed and dotted lines correspond to the numerically accurate solution, NSA, and SBFA, respectively. Solid and dashed lines marked as A in cases (a)–(c) and those marked as B and C in case (a) almost coincide.

nations of cylindrical functions. Calculations of the RCS versus a GP at the fixed frequency require even less CPU time, since a part of the cylindrical functions and corresponding terms in the matrix elements are calculated just once. We carried out such calculations in order to demonstrate the effect of the aperture angle and shell thickness on the RCS.

Several typical plots demonstrating the effect of  $\phi_0^{(1)}$  are shown in Fig. 5 for three values of the normalized frequency,  $k_0\rho_3 = 2.005, 4.01$ , and  $8.007$ . The first of these values corresponds to the second peak of the frequency dependence of RCS in the case of lossy electric coating shown in Fig. 3(a). The second value corresponds to the vicinity of the fourth peak. The third one is located between a higher-frequency minimum and maximum [see Fig. 3(a)]. Rigorous equations (19), (20), and (27) and two approximations, NSA and SBFA, have been used. In line with NSA, the terms  $Q_{nr} \pm P_{nr}, \theta P_{nr} \pm U_{nr}$ , and  $w_{nr}$  ( $n > 0$ ) are calculated after their approximate asymptotic expressions given by (36)–(40). The use of the SBFA leads to analytical solution instead of the matrix equation. The obtained results show that the extrema in the angular dependence of RCS usually correspond to the extrema in the frequency dependence of RCS [for example, compare the cases A and B in Fig. 5(a) with Fig. 3(a)]. The observed correlation occurs for the circular structure with a cutting as well.

Though there is no possibility to reveal the quantitative dependence of the range of validity of NSA or SBFA for arbitrary coating/filling materials and GPs, we have revealed the main factors, which determine these limits, and obtained typical numerical estimates. For example, increase of the structure thickness leads to decrease of the range of the allowed slot angle variation [compare Fig. 5(a) and (b)]. A general trend is worsening of the accuracy provided by these approaches with increasing the relative square of the slot domain and decreasing wavelength in the lossy medium.

In Fig. 5(b) and (c), the relative difference between accurate and approximate values of RCS  $b < 0.1\%$  is observed if  $v = \sqrt{|\varepsilon_1\mu_1|l_\phi}/\lambda_0 \leq 0.65$  and  $b < 1\%$  if  $v \leq 1.15$  where  $l_\phi$  is the linear dimension of the arc corresponding to the slot aperture, and  $\lambda_0$  is the free-space wavelength. Estimates obtained for either a cut cylinder [e.g., in Fig. 5(c)] or slotted thick cylinder [e.g., in Fig. 5(b)] can be used as the majorant estimates for thinner shells. For example, in Fig. 5(a),  $b < 0.1\%$  if  $v \leq 2.25$ . For other materials, the majorant estimates of the range of validity of NSA can be obtained in the same manner, i.e., by comparing the accurate and approximate results obtained for either a cut or slotted thick cylinder. It is worth to compare the above estimates with the range of validity of the large-order asymptotics of cylindrical functions used to derive (36)–(40). It can be

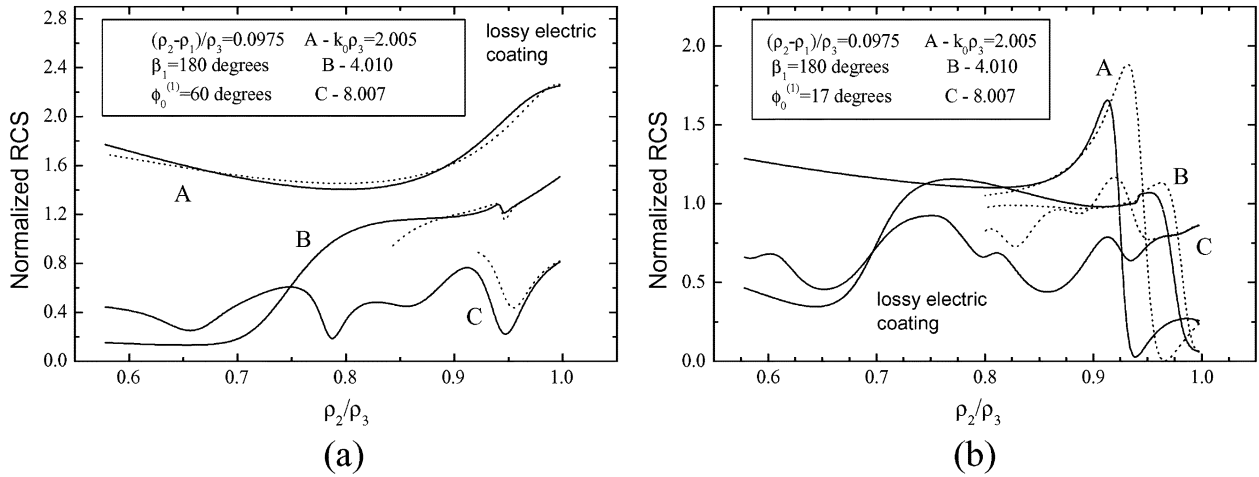


Fig. 6. Dependences of the normalized RCS on the thickness of metallic shell. Structure shows a large opening for (a) and small one for (b) at the symmetric orientation of the slot; it is coated with lossy electric material. Solid and dotted lines correspond to the numerically accurate solution and TWA, respectively.

expressed as  $l_\phi/(\pi\rho_3) \ll 1$ . One can see that NSA can be applied to calculate the slot terms  $Q_{nr} \pm P_{nr}$ ,  $\theta P_{nr} \pm U_{nr}$ , and  $w_{nr}$  at a much weaker limitation.

In the case of SBFA,  $b$ -value is larger than in the case of NSA. Though  $b$  can be 10–20% and higher in some ranges of the angle variation [for example, in vicinity of the minima in Fig. 5(a)], SBFA allows to qualitatively describe behavior of the angle dependence of the RCS in a wide range of  $\phi_0^{(1)}$ -variation (see case A in Fig. 5(a)–(c) and case with  $M = 1$  in Fig. 2). Let assume that SBFA can be used for this purpose if an approximate and accurate curves show the same trend of variation (increase or decrease), and almost the same extrema location and derivative values, while  $b < 5\%$  with the exception of vicinity of the minima. Then the range of possible application of SBFA can roughly be estimated as  $v \leq 0.4$ . For very small thickness as in Fig. 5(a),  $v \leq 0.8$ . In the case of rather large  $\text{Im}|\varepsilon_1\mu_1|$  (e.g., in the case of magnetic coating), this range can be even wider. The same is true with respect to the ranges of 0.1%- and 1%-accuracy if NSA is used.

Now consider the effect of the metallic shell thickness on the RCS. Fig. 6 shows the dependences of the RCS on  $\theta = \rho_2/\rho_3$  obtained with the aid of rigorous equations (19), (20), (27), and the TWA. In the latter case,  $Q_{nr} + P_{nr}$  and  $\theta P_{nr} + U_{nr}$  are given by (33) and (34), while  $Q_{nr} - P_{nr}$  and  $\theta P_{nr} - U_{nr}$  are assumed to be zero. It follows from the obtained results that taking nonzero thickness of the metallic wall into account is especially important if the extrema in the frequency dependence are strongly pronounced [compare Fig. 6(b) with Fig. 4(a)]. The larger  $|d\tilde{\sigma}|/d(k_0\rho_3)$ , the stronger the effect of  $\theta$  on the RCS.

In case of very small thickness,  $1 - \theta < 0.001$ , TWA usually allows one to obtain the results with  $b < 1\%$ . It can also be used for relatively thick shells (say,  $\theta = 0.7 \dots 0.8$ ). However, in this case estimation of the range of its validity is rather complicated. Except for the value of  $k_0(\rho_3 - \rho_2)$ , the presence of the extrema and their locations with respect to each other are the factors, which mainly affect the range of validity of TWA. From the point of view of the TWA application, the worst case is that when a minimum and a maximum on the frequency dependence are located very close to each other [for

example, see  $\theta > 0.9$  in Fig. 6(b)]. TWA can give more accurate results for smaller values of  $\theta$ , while a sharp resonance is observed for larger  $\theta$ . For example, in Fig. 6(b)  $b < 5\%$  at  $0.8 \leq \theta \leq 0.9$ ,  $0.86 \leq \theta \leq 0.96$ , and  $\theta \geq 0.95$  in the cases A, B, and C, respectively. For the parameters used in Fig. 6(a), the resonances of the frequency dependence of RCS are not so sharp and the value of  $k_0(\rho_3 - \rho_2)$  exerts the strongest effect on  $b$ . In this case,  $b < 5\%$  at  $\theta \geq 0.6$ ,  $0.88$ , and  $0.97$  in the cases A, B, and C, respectively. The mentioned features and estimates remain in a wide range of variation of the material parameters and slot angle, at least if  $1 \leq |\varepsilon_1\mu_1| \leq 3.5$  and  $15^\circ \leq \phi_0^{(1)} \leq 60^\circ$ . For larger  $|\varepsilon_1\mu_1|$ , the range of  $\theta$ -variation, in which  $b < 5\%$ , can be substantially narrower. It follows from the obtained results that the calculations can be substantially simplified in a wide range of the variation of GPs and frequency by applying one of the considered approximations. They also allow one to predict the location of maxima of the frequency dependence of RCS even if  $b$  is equal to several per cent.

#### IV. CONCLUSION

In this work, the scattering of the TE-polarized plane wave by a circular slotted cylinder (with and without inner coating) showing nonzero thickness, and by a circular cylinder with a sectorial cutting (with and without filling) has been studied. The theory developed is based on the coupled IEs technique and the Galerkin method with the weighted Gegenbauer polynomials as a basis. The obtained numerical results show quite fast convergence with respect to the number of basis functions and demonstrate the main features of the RCS dependences on frequency, slot/cutting aperture angle, and metallic shell thickness. This approach can be applied to a wide class of CBAs, including the case of very small thickness. Based on the obtained results, we have revealed the situation when the effect of the shell thickness is the strongest and must be taken into account even if the thickness is rather small. This occurs when a minimum and a maximum in the frequency dependence of RCS are located very close to each other.

In addition to numerical study, we have explored the potentials of three approximations of the field in the slots, namely

NSA, SBFA, and TWA. The use of NSA and TWA allows one to replace the combinations of cylindrical functions corresponding to the slot/cutting domain by simple analytical expressions. The most interesting results are obtained with the NSA. The limits of its validity in the RCS calculations are far beyond those for a separate cylindrical function whose argument corresponds to the slot/cutting domain. The revealed correlation between the extrema observed in the dependences of RCS on frequency, aperture angle, and shell thickness also lead to simplification of the analysis.

## REFERENCES

- [1] L. B. Felsen and G. Vecchi, "Wave scattering from slit coupled cylindrical cavities with interior loading: Part II-Resonant mode expansion," *IEEE Trans. Antennas Propag.*, vol. 39, no. 8, pp. 1085–1097, Aug. 1991.
- [2] W.-Y. Yin, L.-W. Li, T.-S. Yeo, and M.-S. Leong, "Multiple penetration of a TEz-polarized plane wave into multilayered cylindrical cavity-backed apertures," *IEEE Trans. Electromagn. Compat.*, vol. 42, no. 4, pp. 330–338, Nov. 2000.
- [3] W.-Y. Yin, L.-W. Li, T.-S. Yeo, M.-S. Leong, and P.-S. Kooi, "The near-zone field characteristics of an E-polarization plane wave penetrating through cylindrical multiple apertures (non) coated with lossy and lossless media," *IEEE Trans. Electromagn. Compat.*, vol. 44, no. 2, pp. 329–337, May 2002.
- [4] A. El-Hajj, K. Y. Kabalan, and R. F. Harrington, "Characteristic modes of a slot in a conducting cylinder and their use for penetration and scattering, TE-case," *IEEE Trans. Antennas Propag.*, vol. 40, no. 2, pp. 156–161, Feb. 1992.
- [5] J. D. Shumpert and C. M. Butler, "Penetration through slots in conducting cylinders: Part 1—TE case," *IEEE Trans. Antennas Propag.*, vol. 46, no. 11, pp. 1612–1621, Nov. 1998.
- [6] ———, "Penetration through slots in conducting cylinders—Part 2: TM case," *IEEE Trans. Antennas Propag.*, vol. 46, no. 11, pp. 1622–1628, Nov. 1998.
- [7] P. M. Goggans and T. M. Shumpert, "Backscatter RCS for TE and TM excitations of dielectric-filled cavity backed apertures in 2-D bodies," *IEEE Trans. Antennas Propag.*, vol. 39, no. 8, pp. 1224–1227, Aug. 1991.
- [8] M. G. Andreasen, "Scattering from parallel metallic cylinders with arbitrary cross sections," *IEEE Trans. Antennas Propag.*, vol. 12, no. 6, pp. 746–754, Nov. 1964.
- [9] J. A. Beren, "Diffraction of an H-polarized electromagnetic wave by a circular cylinder with an infinite axial slot," *IEEE Trans. Antennas Propag.*, vol. 31, no. 5, pp. 419–425, May 1983.
- [10] T. M. Wang, A. Cuevas, and H. Ling, "RCS of a partially open rectangular box in the resonator region," *IEEE Trans. Antennas Propag.*, vol. 38, no. 9, pp. 1498–1504, Sept. 1990.
- [11] Y. C. Noh and S. D. Choi, "TM scattering from hollow slotted circular cylinder with thickness," *IEEE Trans. Antennas Propag.*, vol. 45, no. 5, pp. 909–910, May 1997.
- [12] C. S. Lee and S. W. Lee, "RCS of a coated circular waveguide terminated by a perfect conductor," *IEEE Trans. Antennas Propag.*, vol. 35, no. 4, pp. 391–398, Apr. 1987.
- [13] A. I. Nosich, "Green's function dual series approach in wave scattering by combined resonant scatterers," in *Analytical and Numerical Methods in EM Wave Theory*, M. Hashimoto, M. Imeden, and O. A. Tretyakov, Eds., Tokyo, Japan: Science House, 1993, pp. 419–469.
- [14] W. A. Johnson and R. W. Ziolkowski, "The scattering of an H-polarized plane wave from an axially slotted infinite cylinder: A dual series approach," *Radio Sci.*, vol. 19, no. 1, pp. 275–291, 1984.
- [15] R. W. Ziolkowski and J. B. Grant, "Scattering from cavity-backed apertures: The generalized dual series solution of the concentrically located E-Pol slit cylinder problem," *IEEE Trans. Antennas Propag.*, vol. 35, no. 5, pp. 504–528, May 1987.
- [16] D. Colak, A. Nosich, and A. Altintas, "Radar cross section study of cylindrical cavity-backed apertures with outer or inner material coating: The case of E-polarization," *IEEE Trans. Antennas Propag.*, vol. 41, no. 11, pp. 1551–1559, Nov. 1993.
- [17] ———, "Radar cross-section study of cylindrical cavity-backed apertures with outer or inner material coating: The case of H-polarization," *IEEE Trans. Antennas Propag.*, vol. 43, no. 5, pp. 440–447, May 1995.
- [18] S. Amari, S. Catteux, R. Vahldieck, and J. Bornemann, "Analysis of ridged circular waveguides by the coupled-integral-equations technique," *IEEE Trans. Microwave Theory Tech.*, vol. 46, no. 5, pp. 479–493, May 1998.
- [19] *Handbook of Mathematical Functions*, ser. National Bureau of Standards, Appl. Math. Series, M. Abramovitz and I. A. Stegun, Eds., 1972.
- [20] R. F. Harrington, *Time-Harmonic Electromagnetic Fields*. New York: McGraw-Hill, 1961.
- [21] L. Rayleigh, "Theory of Helmholtz resonator," *Royal Soc. London (A)*, vol. 92, pp. 265–275, 1915.
- [22] A. I. Nosich and V. P. Shestopalov, "An electromagnetic analog of a Helmholtz resonator," *Sov. Phys. Dokl.*, vol. 22, no. 4, pp. 251–253, 1977.



**Andriy E. Serebryannikov** (M'00) was born in Kharkov, Ukraine, in 1967. He graduated from the Physics and Technology Department, Kharkov Polytechnic University and received the Ph.D. degree in radio physics from the Kharkov National University, in 1990 and 1996, respectively.

In 1992, he joined the Institute of Radio Astronomy, National Academy of Sciences of Ukraine, Kharkov. He is currently with the Technische Universität Hamburg-Harburg, Hamburg, Germany. His current research interests include electromagnetic theory of periodic and nonperiodic slotted and rodded structures, inhomogeneous media, theory and applications of metamaterials, and microwave vacuum tubes.



**Alexander I. Nosich** (M'94–SM'95–F'04) was born in Kharkov, Ukraine, in 1953. He received the M.S., Ph.D., and D.Sc. degrees in radio physics from the Kharkov National University in 1975, 1979, and 1990, respectively.

Since 1979, he has been with the Institute of Radio Physics and Electronics, National Academy of Sciences of Ukraine, Kharkov, where he is currently Leading Scientist. Since 1992, he has held a number of guest Fellowships and Professorships in the EU, Japan, Singapore, and Turkey. His research interests include the method of analytical regularization, propagation and scattering of waves in open waveguides, simulation of semiconductor lasers and antennas, and the history of microwaves.

Dr. Nosich was one of the initiators and a technical committee chairman of the international conference series on Mathematical Methods in Electromagnetic Theory (MMET) in 1990. In 1995, he organized an IEEE AP-S Chapter in East Ukraine, the first one in the former USSR. From 2001 to 2003, he represented the Ukraine, Poland, and the Baltic States in the European Microwave Association.